Journal of Applied Polymer Science

A facile strategy to fabricate microencapsulated expandable graphite as a flame-retardant for rigid polyurethane foams

Xiao-Liang Zhang,[1] Hong-Ji Duan,[2] Ding-Xiang Yan,[1] Li-Quan Kang,[3] Wei-Qin Zhang,[1] Jian-Hua Tang,[3] Zhong-Ming Li[1]

[1]College of Polymer Science and Engineering, State Key Laboratory of Polymer Materials Engineering, Sichuan University, Chengdu 610065, People's Republic of China

[2]College of Material Science and Engineering, North University of China, Taiyuan 030051, People's Republic of China

[3]College of Chemical Engineering, Sichuan University, Chengdu 610065, People's Republic of China

Correspondence to: D.-X. Yang (E-mail: yandingxiang@scu.edu.cn) and W.-Q. Zhang (E-mail: zhangwqq@tom.com)

ABSTRACT: A facile strategy is reported for one-step preparation of reactive microencapsulated expandable graphite (EG) for flame-retardant rigid polyurethane foams (RPUF), which is based on *in situ* emulsion polymerization and the use of poly(glycidyl methacrylate) (PGMA) as reactive polymer shell. FTIR and SEM observations well demonstrate the formation of PGMA microencapsulated EG (EG@PGMA) particles. The encapsulation of PGMA shell significantly improves the expandability of EG particles from 42 to 70 mL g^{-1}. RPUF/EG@PGMA composite with only 10 wt % EG@PGMA loading reaches the UL-94 V-0 rating. The limiting oxygen indexes increase remarkably from 21.0 to 27.5 vol %. Additionally, the improved chemical and physical interaction enhance the interfacial bonding between EG and matrix, thus resulting in improved mechanical properties of RPUF/EG@PGMA. These attractive features suggest that the strategy proposed here can serve as a promising means to prepare highly efficient, reactive microencapsulated EG and corresponding good flame-retarding RPUF with high mechanical properties. © 2015 Wiley Periodicals, Inc. J. Appl. Polym. Sci. **2015**, *132*, 42364.

KEYWORDS: flame retardance; foams; polyurethanes

Received 10 March 2015; accepted 13 April 2015

DOI: 10.1002/app.42364

INTRODUCTION

Rigid polyurethane foam (RPUF) has been extensively used in various fields, such as construction, automobile, pipeline, refrigeration, aeronautics, astronautics, etc., where flammability of RPUF is a key issue.[1–4] The most expeditious method used to endow polymer materials with flame retardancy is the incorporation of flame retardants.[5] In recent years, concerns about environmental protection, fire safety, and mechanical properties have put forward new requirements for flame retardants, including nonhalogen, high flame-retarding efficiency, and good compatibility with polymer matrix.

Expandable graphite (EG) is established to be a highly efficient halogen-free flame retardant for RPUF, which suffocates the flame of the composite by generating a voluminous heat insulating layer and protecting the underlying polymer from further decomposition.[6–12] Shi *et al.* reported that, when used as the primary flame retardant, only 10 wt % EG (~200 μm) provided a UL-94 V-0 rating in RPUF/EG composites.[13] Also, there is a synergistic effect between EG and other flame retardants, such as diethyl phosphate,[14] ammonium polyphosphate,[15] aluminum hypophosphite,[16] hollow glass microsphere,[17] whisker silicon oxide,[18] etc., in flame-retarding RPUF. Unfortunately, no matter used along or in combination with synergists, the large-sized EG particles easily caused collapse of some cells and poor interfacial adhesion with RPUF matrix, severely sacrificing the mechanical properties of the RPUF/EG composites.[15,19,20] Although using small-sized EG (~80 μm) could endow RPUF with good mechanical properties, the flame-retardant properties would be deteriorated.[13,21,22] This is because the flame-retardant efficiency of EG depends on its size: more blowing gases will escape from smaller-sized EG flakes before expanding, which results in EG less expandability and thus lower flame-retarding efficiency. Therefore, it is a challenge to find a balance between flame-retardant properties and mechanical properties of RPUF/EG composites.

With regard to the issue for RPUF/EG composites, several methods have been developed, among which microencapsulating EG with polymer shell is affirmed to be an available strategy.[23–26] Microencapsulated EG offers significant advantages

over EG in expandability and interfacial adhesion with RPUF matrix, which is beneficial to both the flame-retardant properties and mechanical properties of RPUF composites. Ye *et al.* prepared poly(methyl methacrylate) (PMMA) microencapsulated EG and activated the PMMA shell via partially hydrolyzing the ester bonds. The RPUF containing 10 wt % microencapsulated particles exhibited a higher limiting oxygen index (LOI) value (26.5 vol %) than that of RPUF/EG (23.5 vol %) and achieved UL-94 V-0 rating. In addition, the compressive strength and modulus of the composites were enhanced considerably to 2.5 and 45.6 MPa from 1.3 and 30.2 MPa, respectively.[24] In order to further enhance the interfacial interaction between EG and RPUF, Zhang *et al.* introduced more reactive groups by using methyl methacrylate-acrylic acid copolymer as the shell materials. The results showed that the mechanical properties were improved dramatically (compressive strength, 2.8 MPa; compressive modulus, 48.4 MPa), and the flame-retardant properties were also enhanced (LOI, 26.0 vol %).[23] However, those methods employed for encapsulating EG always require multistep reactions or multiple monomers. Therefore, it is still a challenging problem to develop a facile route for encapsulating EG with high-reactive polymer shell.

Coating inorganic particles with poly (glycidyl methacrylate) (PGMA) by *in situ* emulsion polymerization to obtain reactive surface has drawn much attention in recent years.[27–29] On one hand, the epoxy groups on PGMA can react with many functional groups such as isocyanate groups, carboxyl, anhydride, hydroxyl, etc.,[30] so that the selection of PGMA as shell material needs no further activation or modification to achieve reactive microencapsulated EG. On the other hand, compared with other encapsulation processes, such as solvent evaporation, heterocoagulation, sol–gel technique, etc., emulsion polymerization is more commonly used for the preparation of microcapsule because of hydro solvent as reacting medium and controllable reaction.

The objective of this work is to provide a facile strategy for fabricating reactive microencapsulated EG for flame-retardant RPUF. To this end, we chose PGMA as functional shell material and *in situ* emulsion polymerization as green encapsulating method. The results indicated that the reactive epoxy groups on PGMA shell were retained and the expandability of the microencapsulated EG (EG@PGMA) increased from 42 to 70 mL g^{-1}. Incorporating EG@PGMA into RPUF made RPUF/EG@PGMA composites pass UL-94 V-0 rating and the LOI values increased to 27.5 vol %. These attractive data were better than those of RPUF/EG composites. Simultaneously, the mechanical properties were also improved because of chemical bonding between PGMA shell and RPUF matrix. Accordingly, the design described in this article keeps a balance between flame-retardant properties and mechanical properties of RPUF/EG composites.

EXPERIMENTAL

Materials

Isocyanate (PAPI, N200) was obtained from Changfeng Chemical Industry (Chongqing, China). Polyether polyol (GR-4110 G) was a product from Gaoqiao Petro. (Shanghai, China). Triethanolamine (TEA), a crosslink catalyst, was purchased from Shanghai Chemical Reagent (Shanghai, China). Dibutyl tin dilaurate (DBTL), a foam catalyst, was supplied by Sichuan Chemical Reagent (Chengdu, China). Expandable graphite (EG, KP9932300) was purchased from Qingdao Haida Graphite (Qingdao, China) and pulverized to −120 mesh (∼80 μm) by an ultrahigh-speed pulverizer. Before used, it was rinsed to neutral with water and dried at 120°C. Glycidyl methacrylate (GMA) was purchased from Nanjing Jiulong Chemical Industry and cleaned up by basic alumina column before used. Potassium persulfate (KPS) as an initiator, sodium dodecyl sulphate (SDS) as an emulsifier, ethanol as a demulsifier, and sodium bicarbonate ($NaHCO_3$) as a buffer were all of analytical grade and supplied by Kelong Chemical (Chengdu, China).

Preparation of EG@PGMA Core–Shell Structure Particles

The reaction was carried out in nitrogen atmosphere. Firstly, 80.0 g EG, 1.0 g SDS, 0.1 g $NaHCO_3$, and 200 mL deionized water were charged into the 500 mL four-necked flask equipped with a mechanical stirrer, thermometer, and condenser in a water bath at 60°C. Then, the mixture was stirred with the mechanical stirrer under the ultrasonic vibration for 1 h. After that 0.2 g KPS was introduced and 10 min later, 40 g GMA was added into the flask in 1 h. Subsequently, the polymerization was held at 60°C for 4 h, and cooled to ambient temperature. After demulsification with ethanol, the product was finally collected by suction filtration and washed thoroughly with water before vacuum dried at 40°C, yielding a gray powder (EG@PGMA).

Pure PGMA was also prepared following the above procedure. Before FTIR, SEM, and TGA test, the residual GMA monomers were extracted from PGMA and EG@PGMA by Soxhlet extraction with methanol. To put it on an equal footing, EG was also purified in the same way.

Foam Preparation

The preparation of the RPUF composites was the same as our previous work.[15,31,32] In this work, the isocyanate index was fixed at 1.1 and the density of the foams was controlled within 0.20 ± 0.02 g cm^{-3}. The content of flame-retardant particles was fixed at 10 wt %. The resultant EG and EG@PGMA filled RPUF composites were abbreviated as RPUF/EG and RPUF/EG@PGMA, respectively.

Measurements

Expanded Volume Testing. The expansion multiple of EG and EG@PGMA particles was measured after expanding at 950 ± 10°C according to GB10698-89.

Horizontal and Vertical Burning Testing. The horizontal and the vertical burning tests were performed with a CTF-2 horizontal and a vertical burning instrument (Jiangning Instruments, China), according to ASTM D 3801-96, and ASTM D 635-98, respectively. The specimens for measurement were machined into sheets of 120 × 13 × 10 mm^3.

Limiting Oxygen Index Testing (LOI). The LOI was measured on an HC-2 oxygen index test instrument (Jiangning Instruments, China) according to ASTM D 2863-09. The dimensions of each sample were 130 × 10 × 10 mm^3.

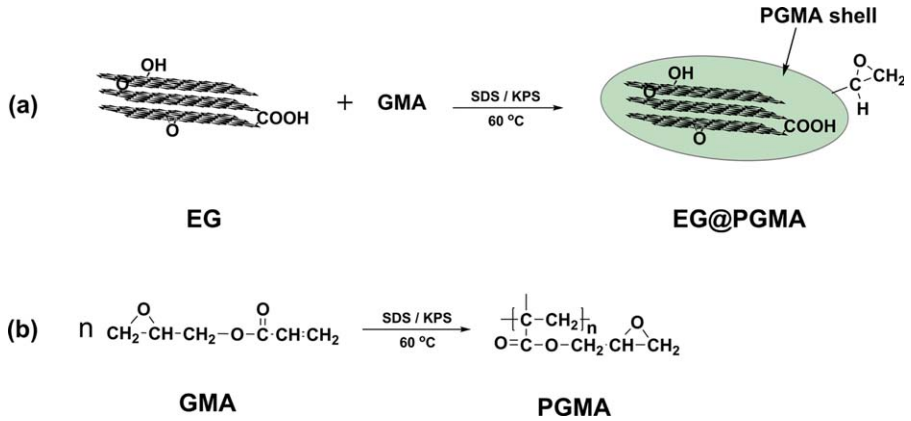

Scheme 1. Synthetic routes of EG@PGMA particles (a) and reaction scheme of the formation of PGMA shell (b). [Color figure can be viewed in the online issue, which is available at wileyonlinelibrary.com.]

Fourier Transform Infrared Spectroscopy (FTIR). FTIR spectrums were recorded on a Nicolet 6700 (Thermo Fisher Scientific, USA) FTIR spectrometer to detect the chemical structure of the core–shell particles. PGMA, EG, and EG@PGMA particles were ground with KBr into fine powders and then pressed the homogeneous mixture into a disk. FTIR spectrums within the wave number range of 400–4000 cm^{-1} were obtained by averaging 32 scans at a resolution of 2 cm^{-1}.

Thermogravimetric Analysis (TGA). TA Instruments Q600 (TA Instruments Inc., USA) was used to determine the amount of PGMA present in the EG@PGMA particles. PGMA, EG, and EG@PGMA particles were ground into fine powder and heated under nitrogen from 50 to 800°C at a heating rate of 10°C min^{-1}.

Scanning Electron Microscopy (SEM). A field-emission SEM Inspect F (FEI, Finland) was utilized to observe the surface of coated and uncoated EG particles and the cross sections of RPUF before and after combustion, which were sputter-coated with gold before observations. The accelerated voltage was held at 20 kV.

Mechanical Property Measurement. The compressive properties under ambient conditions were measured on a universal electronic tensile machine (Shimadzu, Japan) with a compression rate of 3 mm min^{-1} according to ASTM D 1621-10. Specimens in this study have dimensions of 60 × 60 × 30 mm^3 for length, width, and height, respectively.

Dynamic Mechanical Analysis (DMA). A Q800 dynamical mechanical analysis instrument (TA Instruments) was used to analysis the dynamic mechanical properties under air environment. The samples were tested using a three-point bending model at a frequency of 1 Hz and a heating rate of 3°C min^{-1} over a temperature range of 30–250°C. The specimens for measurement were machined into sheets of 40 × 10 × 4 mm^3.

RESULTS AND DISCUSSION

Synthesis and Characterization of EG@PGMA

The mechanism for synthesizing EG@PGMA particles by *in situ* emulsion polymerization with core–shell structure is schematically illustrated in Scheme 1(a), and the reaction scheme of the formation of PGMA shell is presented in Scheme 1(b). When GMA monomers are added dropwise into the reactor, some of them are adsorbed by EG particles, and other monomers form colloidal dispersion in water phase. Under the action of heat, the monomers adsorbed onto the surfaces of the EG particles were initiated and propagated. Meanwhile, the nascent particles from aqueous phase were unstable and adsorbed early on the EG surface, forming a PGMA layer.[33] As shown in Scheme 1(b), a moderate reaction condition (60°C) was adopted to keep the epoxy groups from self-crosslinking, so that as many epoxy groups as possible could be retained.

FTIR was used to further verify the existence of PGMA on the surface of EG particles, as shown in Figure 1. The peaks on the EG pattern match the characteristic bonds of C═C ($\nu_{C=C}$ at 1630 cm^{-1}), and C—O—C (ν_{C-O} at 1220 and 1060 cm^{-1}).[34] The broad peak located at 3430 cm^{-1} can be ascribed to the superposition of O—H stretching vibrations of adsorbed water molecules.[35] In the FTIR of EG@PGMA, the emergence of the significant peaks at 1734 and 1169 cm^{-1} are commonly assigned to the C═O and C—O—C stretching vibration from ester group. Another significant peak at 906 cm^{-1} is associated with

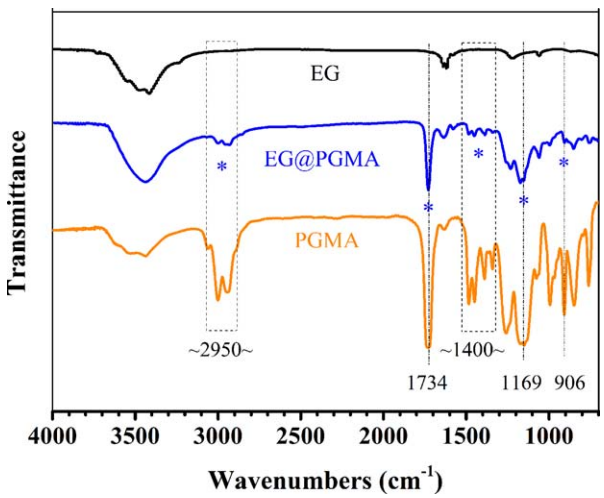

Figure 1. FTIR spectra of EG, PGMA, and EG@PGMA. [Color figure can be viewed in the online issue, which is available at wileyonlinelibrary.com.]

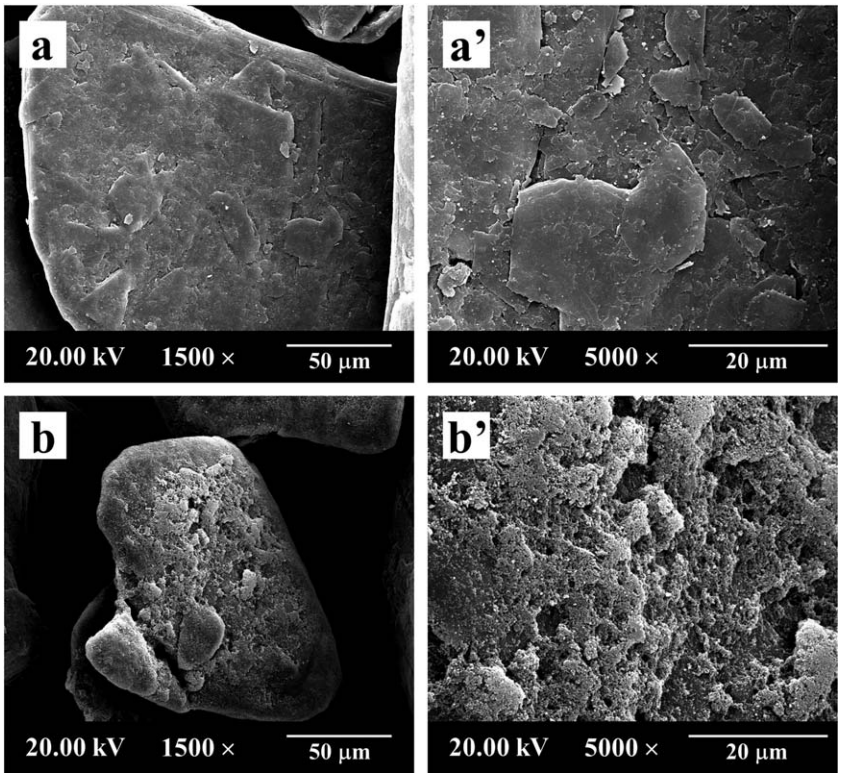

Figure 2. The SEM microphotographs with low and high magnifications: (a) and (a′) EG, (b) and (b′) EG@PGMA.

stretching vibration of the epoxy group.[36,37] Additionally, the peaks ranged from 2943 to 3000 cm^{-1} correspond to the superposition of —CH_2 and —CH_3 asymmetric and symmetric stretching, respectively. Weaker peaks ranged from 1341 to 1484 cm^{-1} are due to —CH_2 and —CH_3 bending.[25,36] All of the characteristic absorption peaks agree with those of pure PGMA, providing evidences for the successful encapsulation of PGMA on EG surface. Furthermore, the results indicate that the above-mentioned experimental conditions are suitable to maintain the epoxy groups which can react with —NCO groups of isocyanate.[38]

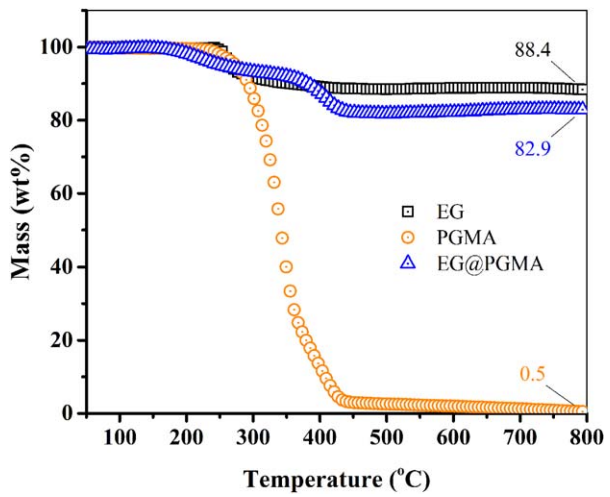

Figure 3. TGA curves of EG, EG@PGMA, and pure PGMA. [Color figure can be viewed in the online issue, which is available at wileyonlinelibrary.com.]

The SEM microphotographs with different magnifications (Figure 2) give a visual interpretation of morphologies of EG and EG@PGMA particles. Clearly, the EG@PGMA particles present rougher surface than the virgin EG particles. A large number of weeny PGMA granules attach to the surface of the EG@PGMA particles and bury the graphite fragments clearly shown on the surface of the EG particles, causing core–shell structure.

TGA curves shown in Figure 3 reveal the thermal behavior of EG, EG@PGMA, and PGMA. It is abstracted that EG@PGMA had two consecutive weight loss steps due to the expansion of particles and the thermal decomposition of PGMA, respectively. While EG exhibits only one weight loss stage because of its expansion. After the heating process, EG owns the highest char yield (88.4 wt %), while almost nothing was left for pure PGMA (0.5 wt %). Compared with EG, EG@PGMA shows less residuals (82.9 wt %) after the analysis, also indicating a successful PGMA coating on EG. The yields of residual carbon can

Table I. Expansion Volume of EG and EG@PGMA

Flame-retardant particles	Expanded volume (mL g^{-1})
EG	42
EG@PGMA	70

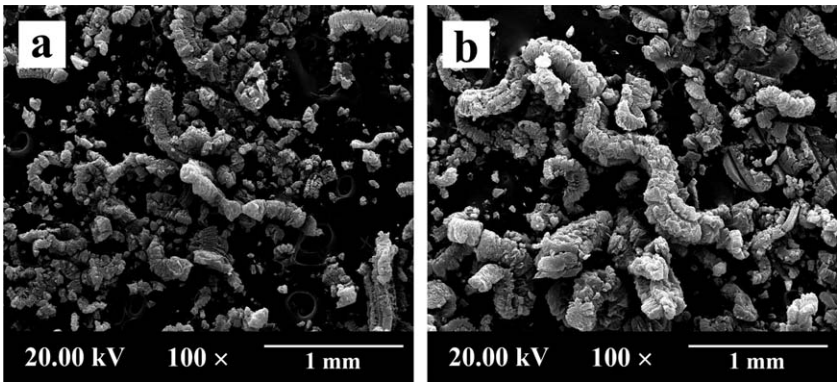

Figure 4. The SEM microphotographs of 'graphite worms: (a) EG, (b) EG@PGMA.

be used to calculate the content of EG and PGMA resin in EG@PGMA particles, according to eqs. (1) and (2)[24]

$$W_{PGMA} = \frac{M_{EG} - M_{EG@PGMA}}{M_{EG} - M_{PGMA}} \times 100\% \quad (1)$$

$$W_{EG} = 100\% - W_{PGMA} \quad (2)$$

where M_{EG}, M_{PGMA}, and $M_{EG@PGMA}$ are the experimental char yields of EG, PGMA, and EG@PGMA particles at 800°C, respectively. W_{EG} and W_{PGMA} are the calculated mass percentages of EG and PGMA in EG@PGMA particles, respectively. Insertion of the experimental values into eqs. (1) and (2) gives the W_{EG}, and W_{PGMA} values of 93.7 and 6.3 wt %, respectively.

Expansion Behavior of EG and EG@PGMA Particles

Table I presents the expansion volume of EG and EG@PGMA particles. The expanded volume increases from 42 for EG to 70 mL g^{-1} for EG@PMGMA. It is commonly believed that the expansion mechanism of EG is based on a redox process between H_2SO_4 and graphite, according to the redox reaction:

$$C + H_2SO_4 \rightarrow CO_2 \uparrow + H_2O \uparrow + SO_2 \uparrow$$

The blowing gases bring out a big increase in the volume on heating. When EG@PGMA particles are subjected to heat, the existence of PGMA shell can prevent the blowing gases from escaping from EG flakes before EG expanded completely, resulting in higher expansion volume than that of EG particles. The improvement in expansion volume can also be established by the morphology of the particles, as shown in Figure 4. The 'graphite worms' formed by EG@PGMA particles are obviously bigger than those of EG particles. Generally, the flame-retardant performance of EG depends on its expandability, i.e., the more expandability, the better flame-retardant performance.[19] Therefore, the encapsulation of PGMA makes EG a highly efficient flame retardant for RPUF. All of the above-mentioned results reveal that the one-step method is an available strategy to fabricate microencapsulated EG with reactive surface and high expansion rate.

Flame-Retardant Properties of RPUF/EG@PGMA

The LOI values and UL-94 classification of pure RPUF, RPUF/EG, and RPUF/EG@PGMA composites are listed in Table II. Owing to the cellular structure and high-level radiant flux, pure RPUF presents a low LOI value of 21.0 vol % and has no rating in the UL-94 horizontal and vertical burn tests, showing poor fire resistance. With 10 wt % EG, RPUF/EG composites pass V-1 rating in vertical burning test and own a LOI value of 25.5 vol %. While for the RPUF/EG@PGMA composites, an enhancement of the flame-retardant properties was obtained. Not only the LOI value increases to 27.5 vol % from the initial value of 21.0 vol %, but also the rating of vertical burning test is promoted to V-0 rating from no rating. The improvement in flame-retardant properties of RPUF/EG@PGMA is mainly attributed to the fact that the EG@PGMA owns bigger expanded volume than EG, and therefore a more efficient carbonaceous layer is formed upon heating. On the other hand, the thermal stability of oxazolidone moieties is higher than that

Table II. Regulation Combustion Test of RPUF/EG@PGMA

		UL-94 horizontal burning test		UL-94 vertical burning test	
Samples	LOI (vol %)	Burring rate (mm/min)	Rating	t_1/t_2[a] (s)	Rating
RPUF	21.0	139.8	NR[b]	BC[c]	NR[b]
RPUF/EG	25.5	-[d]	HB[e]	11.1/6.7	V-1
RPUF/EG@PGMA	27.5	-[d]	HB[e]	4.4/4.6	V-0

[a] t_1 and t_2 (s), average combustion times after the first and second applications of the flame.
[b] NR, no rating.
[c] BC, burns to holding clamp.
[d] Does not pass the 25 mm mark.
[e] HB, cease to burn before the 100 mm reference mark.

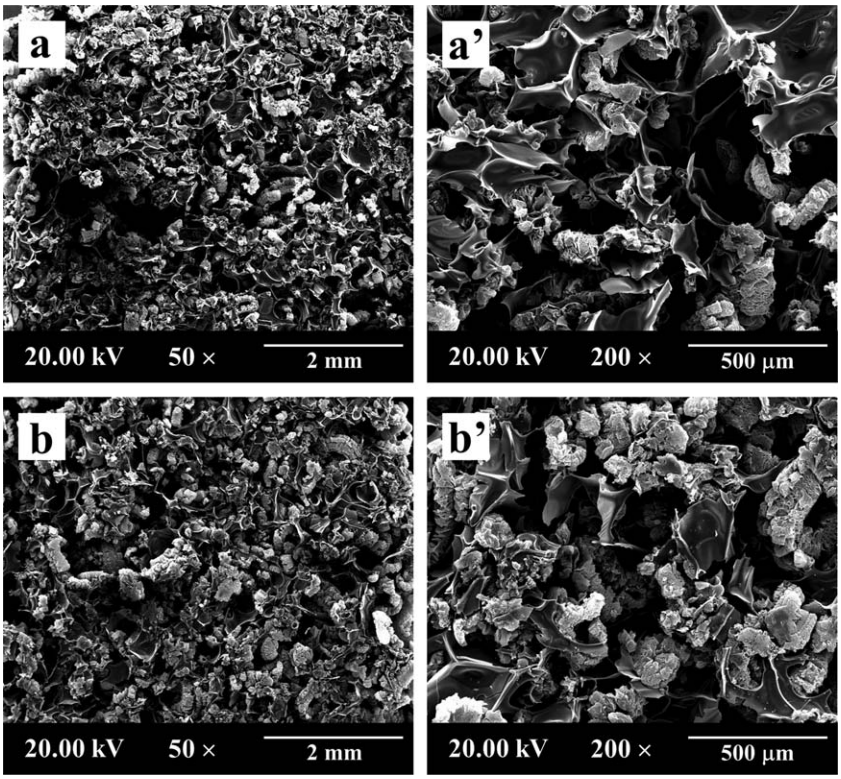

Figure 5. SEM micrographs of the burned char of RPUF composites with low and high magnifications: (a) and (a′) RPUF/EG, (b) and (b′) RPUF/EG@PGMA.

Table III. Compression Performance of RPUF, RPUF/EG, and RPUF/EG@PGMA

Sample ID	Actual density (g cm^{-1})	Compressive strength (MPa)	Compressive modulus (MPa)
RPUF	0.20	2.8	67.2
RPUF/EG	0.21	2.2	45.8
RPUF/EG@PGMA	0.18	2.5	65.9

of urethane groups.[39] Therefore, the incorporation of oxazolidone moieties improves the thermal stability and flame-retardant properties of RPUF/EG@PGMA to some extent.

The SEM micrographs (Figure 5) of char residues of the RPUF composites after flame combustion give a direct interpretation for the different flame-retardant performances of the EG and EG@PGMA particles. The char residues of RPUF/EG, as presented in Figure 5(a, a′), display a small quantity of 'graphite worms' with small size. While for RPUF/EG@PGMA Figure 5(b, b′), a more compact and continuous carbonaceous layer with numerous large-sized 'graphite worms' are formed on the char surface due to the excellent expansion property, explaining the satisfactory flame-retardant performance of RPUF/EG@PGMA. Furthermore, the 'graphite worms' are hardly destroyed by the air current owing to less volatile products. It can be concluded that the shield of PGMA plays a positive role by enhancing the expansion volume of EG facilitating the formation of coherent insulation carbon layer. This well-formed insulation char layer could easily terminate the combustion process and prevent the flammable RPUF matrix from burning,[40] and thus providing RPUF/EG@PGMA with good flame retardancy.

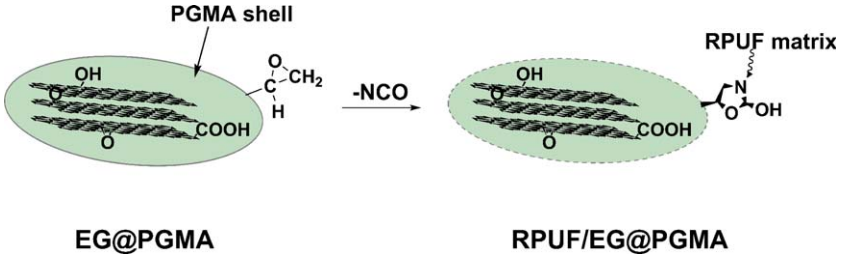

Scheme 2. Schematic representation of the reaction between EG@PGMA composites and –NCO of isocyanate to synthesize RPUF/EG@PGMA. [Color figure can be viewed in the online issue, which is available at wileyonlinelibrary.com.]

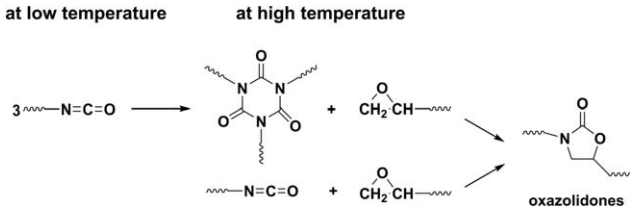

Scheme 3. Detailed chemical reaction scheme of between epoxy group and –NCO of isocyanate.

Compressive Properties of RPUF Composites

In addition to flame-retardant properties, mechanical properties are also important for the application of RPUF. Unfortunately, due to the poor interfacial interaction between EG particles and RPUF matrix, the compressive properties of RPUF were severely sacrificed. As shown in Table III, the compressive strength and compressive modulus of RPUF/EG decrease by 21 and 32%, respectively, compared to that of pure RPUF. However, the compressive strength and compressive modulus of RPUF/EG@PGMA, relative to that of RPUF/EG, are increased to 2.5 and 65.9 MPa from 2.2 and 45.8 MPa, respectively, which are close to that of pure RPUF. The reinforcing mechanism, as illustrated in Scheme 2, is based on the enhanced interfacial bonding between EG@PGMA particles and RPUF matrix. In addition, the improvement of the mechanical properties of RPUF/EG@PGMA can also be attributed to good physical interaction, namely, the wettability of the filler with the initial components.

As per Scheme 3, the epoxy groups on PGMA granules are reactive and can react with the –NCO groups of isocyanate to form oxazolidone moieties.[41] The strong chemical bonds forming during foaming and subsequent crosslinking process and improved physical interaction enhance the interfacial strength between EG@PGMA particles and RPUF matrix, endowing RPUF/EG@PGMA with the satisfactory mechanical properties. When the matrix is subjected to external force, more load can be effectively transferred through the interface from RPUF matrix to the EG particles, therefore the compressive properties of the composite were improved.

To give more details for improved compressive properties of RPUF/EG@PGMA, the SEM morphology of pure RPUF, RPUF/EG, and RPUF/EG@PGMA is displayed in Figure 6. There are no significant changes in cell size and cell structure among pure RPUF, RPUF/EG, and RPUF/EG@PGMA, indicating that the introduction of EG or EG@PGMA particles has little effect on foaming process of RPUF. Nevertheless, high magnification observation shows significant difference at the particles-polymer matrix interface of the composites. Many obvious gaps around the EG particles in RPUF/EG, revealing poor interfacial interaction between the EG particles and matrix. It is interesting that EG particles present very harsh surface after fracturing process, which may be caused by the displacement and deformation of tiny graphite fragments adhering to the EG particles. In contrast, hardly any gaps or cracks are found around the EG@PGMA particles, demonstrating strong interfacial interaction between the EG@PGMA particles and RPUF. Amazingly, owing to the strong adhesion, the EG@PGMA particle is not pulled out but broken in half during fracturing process. All of the evidences indicated that the EG@PGMA particles enhanced the compression performance of RPUF composites.

Dynamic Mechanical Analysis (DMA) of RPUF Composites

DMA can give information about the modifications induced by the introduction of a filler.[42] In this investigation, DMA was used to analyze the viscoelastic properties, including the storage modulus (E') and the loss tangent ($\tan\delta$) which is a measurement of damping. Figure 7(a) shows the temperature dependence of E' for pure RPUF, RPUF/EG, and RPUF/EG@PGMA. All the curves represent the well-known effect of the storage

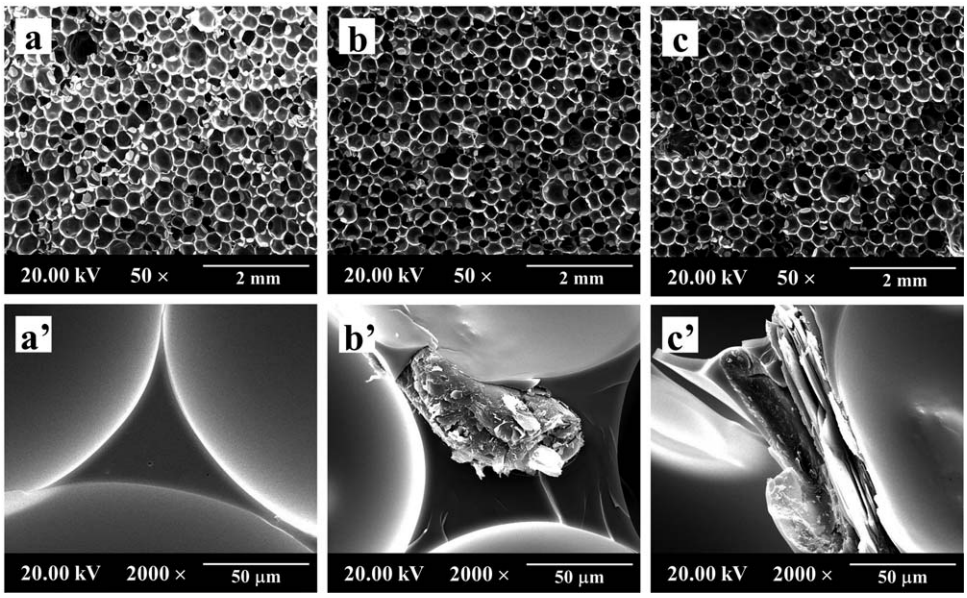

Figure 6. SEM micrographs of RPUF composites with low and high magnifications: (a) and (a′) RPUF, (b) and (b′) RPUF/EG, (c) and (c′) RPUF/EG@PGMA.

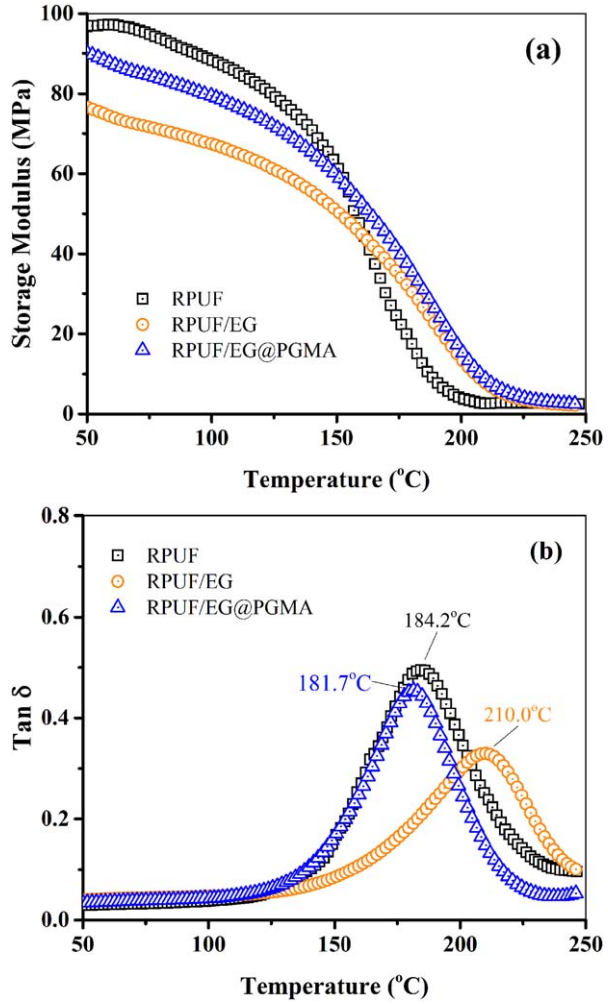

Figure 7. The storage modulus (a) and tanδ (b) of RPUF, RPUF/EG, and RPUF/EG@PGMA. [Color figure can be viewed in the online issue, which is available at wileyonlinelibrary.com.]

modulus fall of nearly two orders of magnitude in the temperature region associated with the glass-transition temperature (T_g). This is because the mobility of the molecular chains increases with the rising of temperature. Compared with RPUF/EG, RPUF/EG@PGMA exhibits higher E' value in the whole temperature range. For example, the E' value at 50°C increases from 76.6 to 90.3 MPa, which is as much as that of pure RPUF (96.8 MPa). The improvement in E' is also attributed to the good adhesion between EG@PGMA and matrix.

Figure 7(b) gives the tanδ curves of all samples. The RPUF/EG shows the highest T_g (210.0°C) and lowest maximal tanδ (0.33) because the rigid filler system limited the mobility of the molecular chains. Interestingly, RPUF/EG@PGMA shows similar T_g (181.7°C) and maximal tanδ (0.45) with that of pure RPUF (184.2°C and 0.49, respectively), which is the result of comprehensive effect of, interaction of RPUF matrix with the filler and crosslinking degree of RPUF matrix. It is believed that PGMA shells have dual effects on the molecular mobility of RPUF matrix. On one hand, the enhancement of interaction of RPUF with EG@PGMA particles will block the movement of molecular chains. On the other hand, the crosslinking degree of RPUF/EG@PGMA is reduced because of the interfacial reaction mentioned above, weakening the interlock of network segment.[43] Therefore, the T_g value and maximal tanδ value of RPUF/EG@PGMA and pure RPUF remain about the same.

CONCLUSIONS

In this paper, a facile strategy was developed for preparation of microencapsulated EG under moderate conditions. PGMA was chosen as active shell material and environmentally friendly emulsion polymerization was adopted in the study. The SEM and FTIR results directly proved that the PGMA coated on the surface of EG particles and the epoxy groups of PGMA are retained. As discussed from the results of TGA, the content of PGMA in EG@PGMA particles is about 6.3 wt %. With PGMA shield, the expandability of EG@PGMA increased dramatically from 42 to 70 mL g^{-1}, meaning that EG@PGMA owns higher flame-retarding efficiency. With 10 wt % microencapsulated EG, RPUF/EG@PGMA displayed more advantageous flame-retardant and mechanical properties relative to RPUF/EG. RPUF/EG@PGMA passed the V-0 rating during the vertical burning test and the LOI values increased from 25.5 to 27.5 vol %. The epoxy groups of PGMA shell would open and react with –NCO to form oxazolidone moieties and simultaneously improve the physical interaction, enhancing the interface strength between EG@PGMA and RPUF matrix. Therefore, the mechanical properties of RPUF/EG@PGMA were increased to an optimal level which was in close proximity to that of pure RPUF. In a word, the one-step method proposed here is a promising strategy to modify EG greenly, which is of important significance to the application of EG in flame-retarding RPUF.

ACKNOWLEDGMENTS

The authors gratefully acknowledge the financial support from the National Natural Science Foundation of China (Grant Nos. 21176158, 51173174, and 51473102).

REFERENCES

1. Qian, L. J.; Feng, F. F.; Tang, S. *Polymer* **2014**, *55*, 95.
2. Wu, C. H.; Chang, C. Y.; Cheng, C. M.; Huang, H. C. *Polym. Degrad. Stabil.* **2003**, *80*, 103.
3. Hirschler, M. M. *Polym. Adv. Technol.* **2008**, *19*, 521.
4. Thirumal, M.; Khastgir, D.; Nando, G. B.; Naik, Y. P.; Singha, N. K. *Polym. Degrad. Stabil.* **2010**, *95*, 1138.
5. Sain, M.; Park, S. H.; Suhara, F.; Law, S. *Polym. Degrad. Stabil.* **2004**, *83*, 363.
6. Thirumal, M.; Khastgir, D.; Singha, N. K.; Manjunath, B. S.; Naik, Y. P. *J. Appl. Polym. Sci.* **2008**, *110*, 2586.
7. Feng, F. F.; Qian, L. J. *Polym. Compos.* **2014**, *35*, 301.
8. Cheng, J. J.; Shi, B. B.; Zhou, F. B.; Chen, X. Y. *J. Appl. Polym. Sci.* **2014**, *131*.
9. Hu, X. M.; Wang, D. M. *J. Appl. Polym. Sci.* **2013**, *129*, 238.
10. Modesti, M.; Lorenzetti, A.; Simioni, F.; Camino, G. *Polym. Degrad. Stabil.* **2002**, *77*, 195.

11. Duquesne, S.; Le Bras, M.; Bourbigot, S.; Delobel, R.; Camino, G.; Eling, B.; Lindsay, C.; Roels, T. *Polym. Degrad. Stabil.* **2001**, *74*, 493.
12. Zatorski, W.; Brzozowski, Z. K.; Kolbrecki, A. *Polym. Degrad. Stabil.* **2008**, *93*, 2071.
13. Shi, L.; Li, Z. M.; Xie, B. H.; Wang, J. H.; Tian, C. R.; Yang, M. B. *Polym. Int.* **2006**, *55*, 862.
14. Zhang, L. Q.; Zhang, M.; Zhou, Y. H.; Hu, L. H. *Polym. Degrad. Stabil.* **2013**, *98*, 2784.
15. Meng, X. Y.; Ye, L.; Zhang, X. G.; Tang, P. M.; Tang, J. H.; Ji, X.; Li, Z. M. *J. Appl. Polym. Sci.* **2009**, *114*, 853.
16. Yang, H. Y.; Wang, X.; Song, L.; Yu, B.; Yuan, Y.; Hu, Y.; Yuen, R. K. K. *Polym. Adv. Technol.* **2014**, *25*, 1034.
17. Bian, X. C.; Tang, J. H.; Li, Z. M. *J. Appl. Polym. Sci.* **2008**, *109*, 1935.
18. Bian, X. C.; Tang, J. H.; Li, Z. M. *J. Appl. Polym. Sci.* **2008**, *110*, 3871.
19. Shi, L.; Li, Z. M.; Yang, M. B.; Yin, B.; Zhou, Q. M.; Tian, C. R.; Wang, J. H. *Polym. Plast. Technol.* **2005**, *44*, 1323.
20. Cheng, J. J.; Shi, B. B.; Zhou, F. B.; Chen, X. Y. *J. Appl. Polym. Sci.* **2014**, *131*, 40253.
21. Luo, W.; Li, Y.; Zou, H.; Liang, M. *RSC Adv.* **2014**, *4*, 37302.
22. Li, Y.; Zou, J.; Zhou, S.; Chen, Y.; Zou, H.; Liang, M.; Luo, W. *J. Appl. Polym. Sci.* **2014**, *131*, 39885.
23. Zhang, X. G.; Ge, L. L.; Zhang, W. Q.; Tang, J. H.; Ye, L.; Li, Z. M. *J. Appl. Polym. Sci.* **2011**, *122*, 932.
24. Ye, L.; Meng, X. Y.; Ji, X.; Li, Z. M.; Tang, J. H. *Polym. Degrad. Stabil.* **2009**, *94*, 971.
25. Han, J. P.; Liang, G. Z.; Gu, A. J.; Ye, J. H.; Zhang, Z. Y.; Yuan, L. *J. Mater. Chem. A* **2013**, *1*, 2169.
26. Wang, B. B.; Hu, S.; Zhao, K. M.; Lu, H. D.; Song, L.; Hu, Y. *Ind. Eng. Chem. Res.* **2011**, *50*, 11476.
27. Lee, I. S.; Cho, M. S.; Choi, H. J. *Polymer* **2005**, *46*, 1317.
28. Oh, J.; Lee, J. H.; Koo, J. C.; Choi, H. R.; Lee, Y.; Kim, T.; Luong, N. D.; Nam, J. D. *J. Mater. Chem.* **2010**, *20*, 9200.
29. Cunningham, V. J.; Alswieleh, A. M.; Thompson, K. L.; Williams, M.; Leggett, G. J.; Armes, S. P.; Musa, O. M. *Macromolecules* **2014**, *47*, 5613.
30. Zeng, Z.; Yu, J.; Guo, Z. X. *J. Polym. Sci. Polym. Chem.* **2004**, *42*, 2253.
31. Duan, H. J.; Kang, H. Q.; Zhang, W. Q.; Ji, X.; Li, Z. M.; Tang, J. H. *Polym. Int.* **2014**, *63*, 72.
32. Ye, L.; Meng, X. Y.; Liu, X. M.; Tang, J. H.; Li, Z. M. *J. Appl. Polym. Sci.* **2009**, *111*, 2372.
33. Cheng, X. J.; Chen, M.; Zhou, S. X.; Wu, L. M. *J. Polym. Sci. Polym. Chem.* **2006**, *44*, 3807.
34. Li, X. H.; Yi, H. B.; Zhang, J. W.; Feng, J.; Li, F. S.; Xue, D. S.; Zhang, H. L.; Peng, Y.; Mellors, N. J. J. *Nanopart. Res.* **2013**, *15*, 1.
35. Bakare, R. A.; Bhan, C.; Raghavan, D. *Biomacromolecules* **2013**, *15*, 423.
36. Hung, C. Y.; Wang, C. C.; Chen, C. Y. *Polymer* **2013**, *54*, 1860.
37. Liu, L.; Zhang, Y. N.; Li, L.; Wang, Z. Z. *Polym. Adv. Technol.* **2011**, *22*, 2403.
38. Sendijarevic, A.; Sendijarevic, V.; Frisch, K. C.; Vlajic, M. J. *Elastom. Plast.* **1991**, *23*, 192.
39. Chattopadhyay, D. K.; Webster, D. C. *Prog. Polym. Sci.* **2009**, *34*, 1068.
40. Modesti, M.; Lorenzetti, A. *Eur. Polym. J.* **2003**, *39*, 263.
41. Merline, J.; Reghunadhan Nair, C.; Gouri, C.; Sadhana, R.; Ninan, K. *Eur. Polym. J.* **2007**, *43*, 3629.
42. Goyanes, S. N.; König, P. G.; Marconi, J. D. *J. Appl. Polym. Sci.* **2003**, *88*, 883.
43. Li, Y.; Mao, S. F. *J. Appl. Polym. Sci.* **1996**, *61*, 2059.